ЖУРНАЛ СТРУКТУРНОЙ ХИМИИ

2016. Том 57, № 1 *Январь – февраль* *С. 59 – 69*

UDC 541.272:548.737

THE CATALYTIC MECHANISM OF CO OXIDATION IN $AlAu_6$ CLUSTERS DETERMINED BY DENSITY FUNCTIONAL THEORY

A. Li, L. Guo, X. An, N. Liu, Z. Cao, W. Li, X. Zheng, Y. Shi, J. Guo, Y. Xi

School of Chemistry and Material Science, School of Modern Arts and Sciences, Shanxi Normal University, Linfen 041004, China
E-mail: gl-guoling@163.com

Received October, 14, 2014 *Revised December, 7, 2014*

We present density functional calculations of O_2 and CO adsorption on an $AlAu_6$ cluster. It is found that in the $AlAu_6$ cluster the active sites would be first occupied by coming O_2 rather than CO due to a more negative binding energy of the former. Furthermore, the catalytic mechanisms of CO oxidation in $AlAu_6$ clusters, which are based on a single CO molecule and double CO molecules, are discussed. This investigation reveals that the reaction of a single CO molecule with the $AlAu_6O_2$ complex has the lowest activation barrier (0.27 eV), which is 0.51 eV lower than that of the pure Au_6^- cluster. For the $AlAu_6O_2(CO)_2$ complex, due to the structural distortion of the $AlAu_6$ cluster, the activation barrier of the determination rate is higher by 0.53 eV than that of the $AlAu_6O_2CO$ complex, which shows that the cooperation effect of the second CO molecule can go against CO oxidation. For the $Al@Au_6O_2(CO)_2$ complex, the activation barrier of the determination rate is lower by 0.07 eV than the path of one CO molecule, which demonstrates that the cooperation effect of the second CO molecule can prompt CO oxidation.

DOI: 10.15372/JSC20160107

K e y w o r d s: CO oxidation, $AlAu_6$ cluster, catalytic mechanism.

INTRODUCTION

Gold nanoparticles have attracted public attention since the pioneering discovery that Au can exhibit a surprisingly high catalytic activity [1] when it is highly dispersed on certain catalyst supports. Pure and supported Au clusters and nanoparticles have now become one of the most promising catalysts for many important chemical reactions at low temperatures, such as CO oxidation [2—4], the water-gas shift reaction [5, 6], the formic acid oxidation reaction [7], and organic synthesis [8]. In the last years, a number of series of experimental and theoretical works have been devoted to the studies of gold-containing bimetallic clusters [8—15]. Zhu *et al*. found that the catalyst performance of Au—Pd alloy nanoparticles supported by ZrO_2 [8] could be enhanced by light illumination. Kuang [9] and Mao [10] studied the neutral and anion geometries of $Au_nAl^{0/-}$ clusters using the PW91 functional with up to ten atoms. The research revealed that the equilibrium geometries of Au_nAl are three-dimensional for $n \geq 4$, which is different from pure gold clusters. It is worth pointing out that the Al atom prefers to lie in the center rather than on the surface in each the ground state of Au_nAl ($1 \leq n \leq 9$) clusters. Their calculated results also show that there is a similar odd-even alternative phenomenon for energies, second-order energy differences, highest occupied molecular orbital (HOMO)-lowest unoccupied molecular orbital (LUMO) energy gaps, and magnetic moments. Majumder *et al.* [11] have studied the optimized geometries and electronic structures of Au_5M (M = Na, Mg, Al, Si, P, and S)

clusters using the generalized gradient approximation (GGA). The lowest energy isomer of the Au_5Al cluster with the C_{4v} point group symmetry can be seen as a square pyramidal subunit with the fifth Au atom connected to the Al atom at the top. Zhang *et al*. investigated the structures and electronic properties of $M@Au_6$ (M = Al, Si, P, S, Cl, Ar) clusters [12] using the Perdew-Burke-Ernzerhof hybrid functional (PBE). They found that all the ground-state structures of the $M@Au_6$ clusters prefered the low symmetry structures, which is very different to 3*d* transition-metal impurity doped Au_6 clusters. Luo *et al*. have investigated the geometrical structures, growth pattern behaviors, relative stabilities, and electronic properties of Au_nM clusters (M = Al, Si, P, S, Cl; n = 2—8) [13] using density functional theory (DFT) at the PBE level. The geometries, stabilities, and electronic properties of $Au_{12}M$ (M = Na, Mg, Al, Si, P, S, Cl) clusters [14] were researched using Becke′s three-parameter hybrid exchange functional with the LYP correlation functional (B3LYP). This article reveals that the lowest-energy geometries of $Au_{12}Al$ form a cage structure with the Al atom encapsulated in the center of the Au_{12} cluster. There is no doubt that the introduction of an impurity atom into the gold clusters not only induces changes in the geometric and electronic properties, but also strongly influences the physical and chemical properties of host gold systems. Therefore, it is necessary to understand the mechanisms by which these catalysts carry out oxidation reactions.

CO or O_2 adsorption on pure or doped gold clusters has also been investigated both experimentally and theoretically [16—22]. Nhat and co-workers reported Au_nV—CO complexes [16]. Compared with the pure gold clusters, V-doped gold clusters Au_nV are more effective for CO adsorption. For Au_nV—CO, it is found that CO adsorption at the V site is much stronger than that at the Au sites for small Au_nV clusters. However, for large clusters, the V atom is completely encompassed inside the gold cage, so CO is adsorbed on the Au atom. Furthermore, Au_nV—CO complexes have higher CO binding energies and CO frequency shifts than those in the Au_{n+1}—CO complexes, which can be interpreted that with partially filled *d* orbitals vanadium is more inclined to undergo an interaction with either HOMO or LUMO of CO. Lin *et al*. investigated CO adsorption on Au_nY (n = 1—9) clusters [17]. The study reveals that the elongations of the C—O bond length are nearly linear with the red-shifted CO frequency. They also found the CO binding energies and CO frequencies of Au_nYCO were smaller than those of $Au_{n+1}CO$ complexes (except Au_5Y), and the net charge of CO on Au_nYCO is more negative than that on $Au_{n+1}CO$. Wallace *et al*. reported CO and O_2 coadsorption on the Au_6^- cluster [18]. They found that Au_6^- had a high catalytic activity in CO oxidation at room temperature. Sun *et al*. [20] studied O_2 adsorption on Au_n (n = 1, 2, 4, 6) cluster anions using ultraviolet photoelectron spectroscopy (UPS) and DFT calculations. Their investigation revealed that additional charge could be increased in the interaction of O_2 and the Au cluster. Fernández *et al*. [21] studied the CO and O_2 adsorption properties on neutral gold clusters containing from 5 to 10 atoms using the PBE functional. Amft et al. [22] investigated CO and O_2 adsorption on 2D and 3D Au_{13} clusters.

In the past decade, many experimental [2—4] and theoretical [23—26] studies on the catalytic mechanism of CO oxidation have been reported. Gold nanoparticles supported by ZnO nanorods [3] were characterized based on the results of structural and spectroscopic studies. The catalyst shows the encapsulation of gold nanoparticles by ZnO and the electron transfer between gold and the support. Wang *et al*. [23] completed the mechanism of CO oxidation on $Au_3^{0/\pm1}$ clusters using DFT. An *et al*. [24] investigated the reaction mechanism of CO oxidation catalyzed in the helical Au(5,3) nanotube using DFT, and found that the Au(5,3) nanotube exhibited a high catalytic activity for CO oxidation. CO oxidation exhibits complex behavior depending on support-induced charge states controlled by support vacancies. Stamatakis *et al*. [25] investigated the CO oxidation mechanism on MgO-supported Au_6 clusters by combining for the first time DFT calculations with graph theoretical kinetic Monte Carlo (KMC) simulations. In addition, a large amount of investigations have been performed on the catalytic mechanism of CO combustion by bimetallic clusters [27—29]. The catalytic properties of Ag_xAu_{3-x}/MgO (100) clusters in CO oxidation [29] were studied by Negreiros *et al*. using DFT.

Even though the geometric and electronic properties of $AlAu_6$ clusters have been reported, they have not been studied with respect to CO adsorption and the catalytic mechanism of CO combustion on them. In this paper, we investigate the structures of O_2 and CO adsorption on the $AlAu_6$ cluster. The main objective of this study is to present the catalytic mechanism of CO oxidation by $AlAu_6$ clusters.

METHODOLOGY AND COMPUTATIONAL DETAILS

The calculations are performed using the Gaussian03 program [30]. Full optimization of the structures and frequencies is carried out using density functional theory (DFT) by the unrestricted DFT method with the general gradient approximation (GGA) in the form of the Perdew—Burke—Ernzerhof (PBE) [31] functional.

Mixed 6-31G* and LANL2DZ basis sets were employed. An all-electron 6-31G* basis set was used for Al, C, and O atoms. The LANL2DZ pseudo-potential is adopted for valence electrons of the Au atom, and its core electrons are represented by the LANL2DZ effective core potential (ECP). This scheme is a good compromise between the accuracy and the computational efficiency. Its application has been shown to be effective for the Au_nM [10] system. All of the vibrational frequencies have been calculated using the analytic evaluation of the second energy derivatives to judge whether the structure was the local minimum. All reported geometries reflect stable minima on their respective potential energy surfaces with no imaginary frequencies. The natural bond orbital (NBO) charges of atoms are computed to understand charge transfers in the interaction. The quadratic synchronous transit (QST) method [32] is used to determine the transition state (TS) geometries. All the structures are fully optimized without any constraints. For reaction pathways, the minima are connected to each TS by tracing the intrinsic reaction coordinate (IRC) [33, 34]. In addition, we also calculated the density of states (DOS) using the CASTEP module [35] of Material Studio [36].

RESULTS AND DISCUSSION

In order to test the reliability of our calculation, Au_2, Al_2, and AlAu dimers are calculated. The results are summarized in Table 1. Furthermore, the calculated bond lengths and binding energies of O_2, CO, and CO_2 are compared with the experimental values. As illustrated in Table 1, our results are in good agreement with previous experimental and theoretical data.

Firstly, the geometric structures of $AlAu_6$ [10] are re-optimized using the PBE functional and are shown in Fig. 1. In contrast to the Au_7 cluster [44], which exhibits the planar structure, the $AlAu_6$

Table 1

Calculated bond lengths, averaged binding energies, and vertical ionization potential, experimental results and theoretical study of this work

Parameter	Ref.	Au_2	Al_2	AlAu	O_2	CO	CO_2
Bond length, Å	This work	2.551	2.497	2.400	1.23	1.15	1.18
	Experimental	2.472[a]	2.560[b]	2.339[c]	1.21[d]	1.13[d]	1.16[d]
E_b, eV	This work	1.080	0.806	1.747	3.12	5.74	5.91
	Experimental	1.14±0.01[a]	0.997±0.108[b]	1.670±0.009[c]	2.62[d]	5.61[d]	5.69[d]
Ionization potential, eV	This work	9.525	6.060	8.036	12.24	13.72	13.39
	Experimental	9.20±0.21[a]	6.200±0.200[b]	—	12.06[e]	14.01[e]	13.77[e]

[a] References [37, 38], [b] [39], [c] [40], [d] [41, 42],[e] [43].

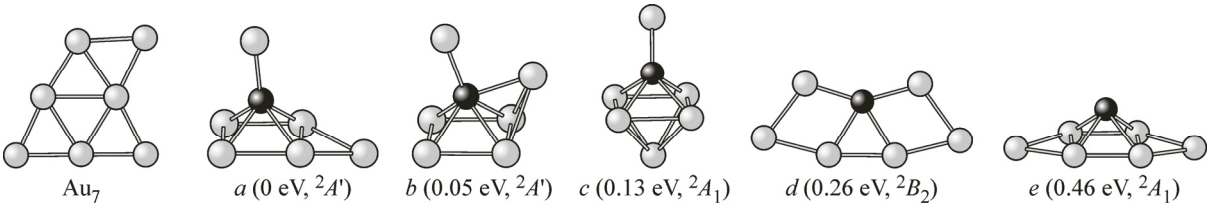

Fig. 1. Lowest-energy (*a*) and low-lying structures of the $AlAu_6$ cluster (*b*). The corresponding energy and electronic states of the complexes are consigned in parenthesis

cluster is three-dimensional. We found that the Al atom preferred to sit inside the Au_6 cluster, forming a higher coordinated rather than a low-lying structure (Fig. 1, *e*) of the Al atom position upside the Au_6 cluster. The lowest-energy structure (Fig. 1, *a*) of $AlAu_6$ has the C_s symmetry, which is different from the structure of the 3D quadrilateral pyramid with the C_{4v} symmetry in [13]. This is due to different basis sets selected.

Furthermore, we studied the adsorption behavior of O_2 and CO on the $AlAu_6$ cluster. Different binding sites are considered for O_2 adsorption on the $AlAu_6$ cluster. For CO adsorption steps, we considered several different orientations (with C or O ends towards the cluster). Further, different possible spin states are considered for clusters with O_2 and CO adsorption. For all isomers of each cluster, the local minima on the potential energy surface are guaranteed by the harmonic vibration frequencies without imaginary modes. The binding energy (BE) is calculated as $BE = E(AlAu_6^-M) - E(M) - E(AlAu_6)$, and the M represents O_2 or CO.

Adsorption of O_2 molecule on $AlAu_6$ clusters. The lowest-energy and low-lying structures and relative energies of $AlAu_6O_2^*$ and $Al@Au_6O_2$ complexes are shown in Fig. 2, *a*. Table 2 presents more details of the geometries, binding energies, and the electronic properties of the complexes.

Fig. 2, *a* shows that the $AlAu_6$ cluster prefers the structure with an O_2 molecule bound to the Al atom. The $AlAu_6O_2^*$ (C_1) is obtained by adding O_2 in the low-lying structure of $AlAu_6$ (Fig. 1, *e*). The O—O bond distance increased to 1.407 Å, which is 0.178 Å longer than that of the free molecule. The O—O vibrational frequency decreased from 1577 cm^{-1} in isolation to 990 cm^{-1}. These facts reveal that the oxygen molecule is activated by the $AlAu_6$ cluster. The binding energy of the $AlAu_6O_2^*$ complex is –1.426 eV and it is more stable than $Al@Au_6O_2$ (–0.967 eV). For $Al@Au_6O_2$, O_2 is adsorbed in the

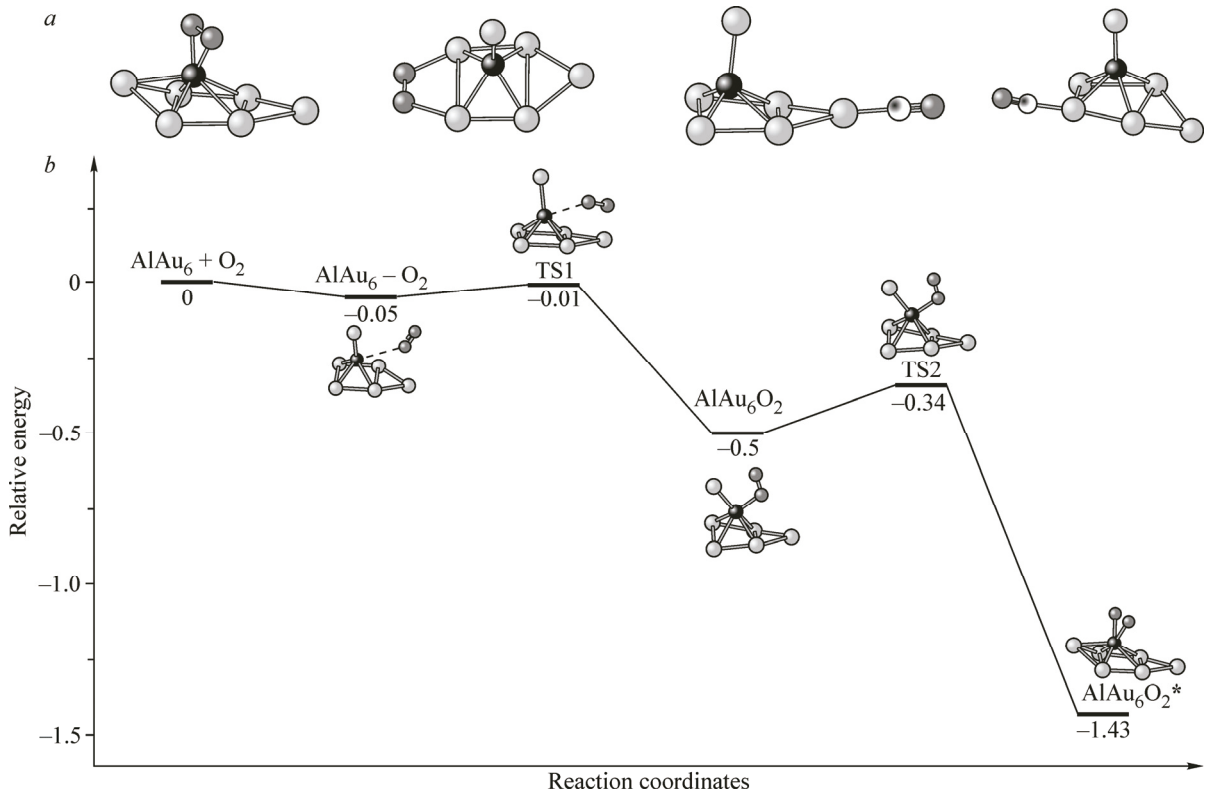

Fig. 2. Two lowest energy optimized structures of O_2 adsorption onto the $AlAu_6$ cluster and two lowest energy optimized structures of CO adsorption onto the $AlAu_6$ cluster (*a*). The most stable structure is labeled with an asterisks (*) symbol. The corresponding energy and electronic states of the complexes are consigned in parenthesis. Oxygen dissociation of via the reaction path: $AlAu_6$—$O_2 \rightarrow$ TS1 $\rightarrow AlAu_6O_2 \rightarrow$ TS2 $\rightarrow AlAu_6O_2^*$ (*b*)

Table 2

Spin multiplicity (M), *binding energies* (BE), *bond distances* (*d*) *of the adsorbates*, *vibrational frequencies and NBO charges of the adsorbates for* $AlAu_6O_2$ *and* $AlAu_6CO$ *clusters represented in Fig*. 1

Complexe	M	BE(O_2), eV	$d_{O—O}$, Å	$\nu_{O—O}$, cm^{-1}	Δq_{O_2}	Complexe	M	BE(CO), eV	$d_{C—O}$, Å	$\nu_{C—O}$, cm^{-1}	Δq_{CO}
$AlAu_6O_2^*$	2	–1.426	1.407	990	–0.706	$AlAu_6CO$*	2	–1.060	1.158	2058	–0.067
$Al@Au_6O_2$	2	–0.967	1.307	1165	–0.210	$AlAu_6CO$	2	–0.825	1.152	2097	0.008

bridging position with two Au atoms. The O—O bond distance is 1.307 Å, which is between that of $AlAu_6O_2^*$ (1.407 Å) and the isolated one (1.229 Å). The O—O vibrational frequency in $Al@Au_6O_2$ is 1165 cm^{-1}, which is larger than that in the $AlAu_6O_2^*$ complex (990 cm^{-1}). These facts indicate that O_2 molecule adsorption on the Al atom is more activated than that on the Au atom. In comparison with pure Au_n (n = 5—10) clusters [21], Al doping can enhance the O_2 absorption. It is found that the red shift of the O—O stretching frequency upon adsorption correlates linearly with the elongation of the O—O bond, which is consistent with the O_2 activation upon adsorption.

According to the NBO charge analysis, the net charge of adsorbed O_2 in $AlAu_6O_2^*$ and $Al@Au_6O_2$ complexes are computed to be –0.706 and –0.210, respectively. This reflects that there is charge transfer from $AlAu_6$ to adsorbed O_2, therefore O_2 acts as an electron acceptor. It is found that the O—O bond elongation and stretching frequency correlate with the charge transfer, which is due to the fact that the metal-to-oxygen back donation increases the π^* orbital population causing the weakening of the O—O bond. In short, the O_2 molecule prefers to bind to the Al site rather than to Au sites. It is worth noting that the linear correlation can be established among the binding energy, the C—O bond extension, a decrease in the C—O vibrational frequency, and charge transfer from the cluster to O_2.

From Fig. 2, *b*, we can see the reaction pathway for O_2 dissociation adsorption on the $AlAu_6$ cluster. TS1 and TS2 are the respective transition state geometries for the $AlAu_6O_2$ formation and the lowest energy $AlAu_6O_2^*$ products from corresponding AlAu-O_2 and $AlAu_6O_2$. The result shows that there is a shallow physisorption with an adsorption energy of 0.05 eV. We label the physisorbed state as AlAu-O_2. In AlAu-O_2 configuration, the oxygen molecule is 3.58 Å away from the Al atom. After passing through TS (TS1, ΔE = 0.04 eV), it reaches the chemisorbed local minimum state $AlAu_6O_2$. The adsorption energy of $AlAu_6O_2$ is 0.57 eV. In TS, the oxygen molecule is 3.08 Å away from the Al atom. These two long bond lengths suggest that the interaction between the gaseous oxygen molecule and the $AlAu_6$ cluster for both physisorbed state and TS (TS1) are the van der Waals interaction in nature. For the $AlAu_6O_2$ complex, the O—O and O—Al distances are 1.32 Å and 1.94 Å, respectively. Then, the adsorption system overcomes the TS energy barrier (TS2, ΔE = 0.16 eV), and reaches the next low chemisorption state ($AlAu_6O_2^*$). In the $AlAu_6O_2^*$ configuration, both oxygen atoms are at 1.88 Å from the Al atom.

Adsorption of a CO molecule on the $AlAu_6$ cluster. In the lowest energy structure of the $AlAu_6CO$* complex (Fig. 2), CO prefers to bind to the Au atom through the C atom. The binding energy of the $AlAu_6CO$* complex is –1.060 eV. The C—O length extends from 1.149 Å of the isolated molecule to 1.158 Å. At the same time, the C—O stretching vibrational frequency in $AlAu_6CO$* is 2058 cm^{-1}, which is smaller than that in isolated CO (2124 cm^{-1}). For the $AlAu_6CO$ complex, the binding energy is –0.825 eV. The C—O length is 1.152 Å, which is larger than that in the isolated molecule (1.149 Å). Furthermore, the C—O vibrational frequency is 2097 cm^{-1}. It is found that the binding energy, the extended C—O length, and a decrease in the C—O vibrational frequency have linear correlation.

The net charge of adsorbed CO in $AlAu_6CO$* and $AlAu_6CO$ complexes are computed to be –0.067 and +0.008, respectively. This is attributed to the complicated mechanism of CO binding with

the $AlAu_6$ cluster. It can be explained by the Blyholder model [45], which describes the metal—CO bonding as donor—acceptor interactions. According to the NBO charge analysis, the Au—CO bond of $AlAu_6CO$* is formed by charge transfer from $AlAu_6$ clusters to CO π^*_{2p} antibonding orbitals, which enhances the Au—CO bond and weakens the C—O bond. This is clearly reflected in the CO vibrational frequency (Table 2). For $AlAu_6CO$, adsorbed CO is positively charged, so CO acts as an electron donor. This can be illustrated by electron transfer from the CO lone pair to the $AlAu_6$ cluster.

Above all, the active sites in the $AlAu_6$ cluster would be first occupied by the coming O_2 rather than CO due to its more negative BE than that of CO.

The catalytic mechanism of CO oxidation on $AlAu_6$ clusters. Two different pathways for CO have been considered in the present work. Two reaction mechanisms are known: the Langmuir—Hinshelwood (LH) and the Eley—Rideal (ER). Prior studies reveal that the LH reaction is proposed to be most probable mechanism of CO oxidation [30—32]. And our paths 1 and 2 also occur via this mechanism. In addition, we consider two reactants: O_2 binding with the Al atom ($AlAu_6O_2$—CO) and O_2 attachment to the Au atom (Al@Au_6O_2—CO). To search for the minimum-energy pathway for CO oxidation, we calculated the doublet potential energy surfaces (PESs) for the reaction promoted by $AlAu_6O_2$ and Al@Au_6O_2. Fig. 3 shows the energy profiles and the geometries of the minima and TSs along each path.

The catalytic mechanism of CO with the $AlAu_6O_2^*$ complex. Fig. 3, *a* shows the calculated PES profiles with the optimized geometries of the stationary points. For the $AlAu_6O_2^*$ complex, the LH mechanism of path-1 starts from CO+O_2 coadsoption forming the structure of IM1, with an adsorption energy of –1.86 eV. Then adsorbed CO can approach and bind through its C atom to the adsorbed O_2 via $TS_{1/2}$ (E_a = 0.27 eV), forming more stable $AlAu_6O$—OCO (IM2). In the next desorption path, via $TS_{2/3}$ (E_a = 0.13e V), from $AlAu_6O$—OCO (IM2) to $AlAu_6O$+CO_2 (IM3), it involves the scission of one C—Au bonds, and this process is exothermic (4.27 eV). After the first CO_2 molecule is desorbed from the nanoparticle, the second CO molecule can react with the $AlAu_6O$ complex. Therefore, CO oxidation proceeds through the formation of OCO by associating the O atom and the CO molecule via $TS_{4/5}$ (E_a = 0.05 eV). Finally, the $AlAu_6CO_2$ complex is produced, requiring an energy of 0.19 eV. It can disaggregate into $AlAu_6$ and CO_2, indicating the accomplishment of the reaction. As a result, the overall reaction

$$AlAu_6 + O_{2(gas)} + CO_{(gas)} \rightarrow AlAu_6^-O_{2(ads)} + CO_{(ads)} \rightarrow AlAu_6O\text{—}OCO \rightarrow AlAu_6^-O_{(ads)} +$$

$$+ CO_{2(gas)} \rightarrow AlAu_6^-O_{(ads)} + CO_{(gas)} + CO_{2(gas)} \rightarrow AlAu_6^-OCO + CO_{2(gas)} \rightarrow AlAu_6 + 2CO_{2(gas)}$$

is thus calculated to be exothermic (6.37 eV).

For the LH mechanism of path-2, we design the cooperative oxidation of two CO molecules on $AlAu_6O_2^*$. From Fig. 3, *a* it follows that two CO molecules approach two Au atoms of the opposite site forming IM6. Then one adsorbed CO molecule can approach and bind through its C atom to adsorbed O_2 via $TS_{6/7}$ (E_a = 0.80 eV), forming more stable IM7. At this step, because of distorting the $AlAu_6$ cluster, the activation barrier (0.80 eV) from IM6 to IM7 is larger than $TS_{1/2}$ (0.27 eV). The next step is the transformation of IM7 into IM8; one CO_2 is formed via $TS_{7/8}$ (E_a = 0.24 eV). Then another CO molecule approaches the O atom via $TS_{8/9}$ (E_a = 0.59 eV), forming $AlAu_6OCO$+CO_2 (IM9). Finally, the $AlAu_6^-(CO_2)_2$ complex with CO_2 can disaggregate into $AlAu_6$ and 2 CO_2, indicating the accomplishment of the reaction; it requires an energy of 0.28 eV. The overall reaction is calculated to be exothermic (6.37 eV).

The catalytic mechanism of CO with the Al@Au_6O_2 complex. Fig. 3, *b* shows the calculated PES profiles with the optimized geometries of the stationary points. For the Al@Au_6O_2 complex, the LH mechanism of path-1 starts from CO+O_2 coadsoption, forming the structure of IM1, with an adsorption energy of –1.44 eV. Then adsorbed CO can approach and bind through its C atom to adsorbed O_2 via $TS_{1/2}$ (E_a = 0.13 eV), forming more stable Al@Au_6O—OCO (IM2). In the next desorption path, via $TS_{2/3}$ (E_a = 0.51 eV), from Al@Au_6O—OCO (IM2) to Al@Au_6O+CO_2 (IM3), it involves the scission of one C—Au bond, and this process is exothermic (2.98 eV). After the first CO_2 molecule is de-

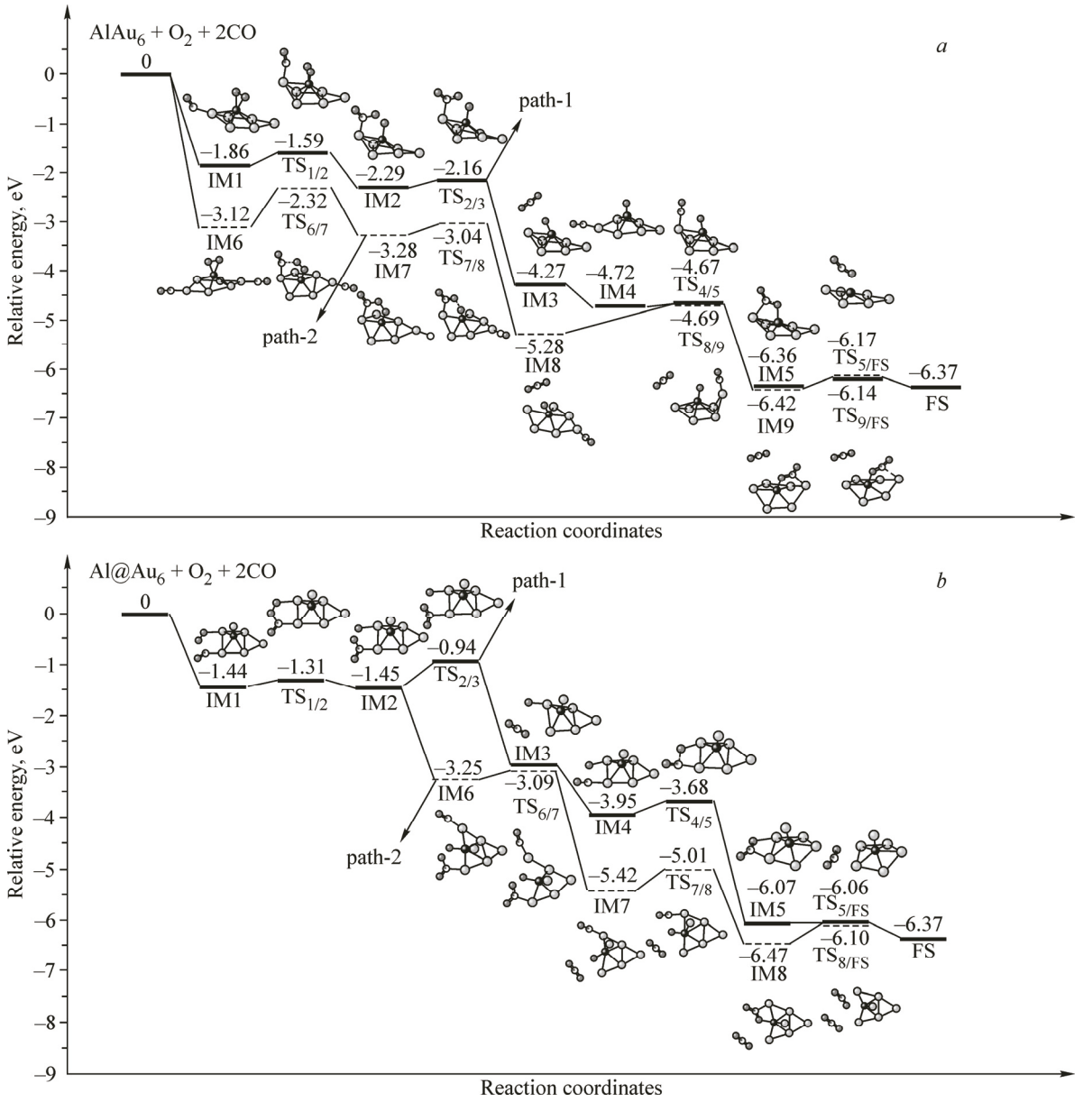

Fig. 3. Energy diagrams of the most favorable pathways of CO oxidations on the $AlAu_6$ cluster (*a*—*b*). CO oxidation involve two CO molecules

sorbed from the nanoparticle, the second CO molecule can react with the $AlAu_6O$ complex. Therefore CO oxidation proceeds to form OCO by associating the O atom and the CO molecule via $TS_{4/5}$ (E_a = 0.27 eV). Finally, the $Al@Au_6CO_2$ complex is produced, requiring an energy of 0.01 eV. It can disaggregate into $AlAu_6$ and CO_2, indicating the accomplishment of the reaction. As a result, the overall reaction is thus calculated to be exothermic (6.37 eV).

The LH mechanism of path-2 involves the cooperative oxidation of two CO molecules on $Al@Au_6O_2$. From Fig. 3, *b* it follows that another CO molecule approaches the Au atom of IM2 forming IM6. At this step, one O atom passes from the Au atom to the Al atom. Then first CO_2 is formed via $TS_{6/7}$ (E_a = 0.16 eV) from $Al@Au_6O$—OCO+CO (IM6) to $Al@Au_6O$—CO+CO_2 (IM7); it involves the scission of one C—Au bond. The next step is to transform IM7 into IM8. Another CO molecule approaches the O atom, forming $Al@Au_6OCO+CO_2$ (IM8) via $TS_{7/8}$ (E_a = 0.41 eV). Finally, the $Al@Au_6^-(CO_2)_2$ complex with CO_2 can disaggregate into $AlAu_6$ and $2CO_2$, indicating the accomplish-

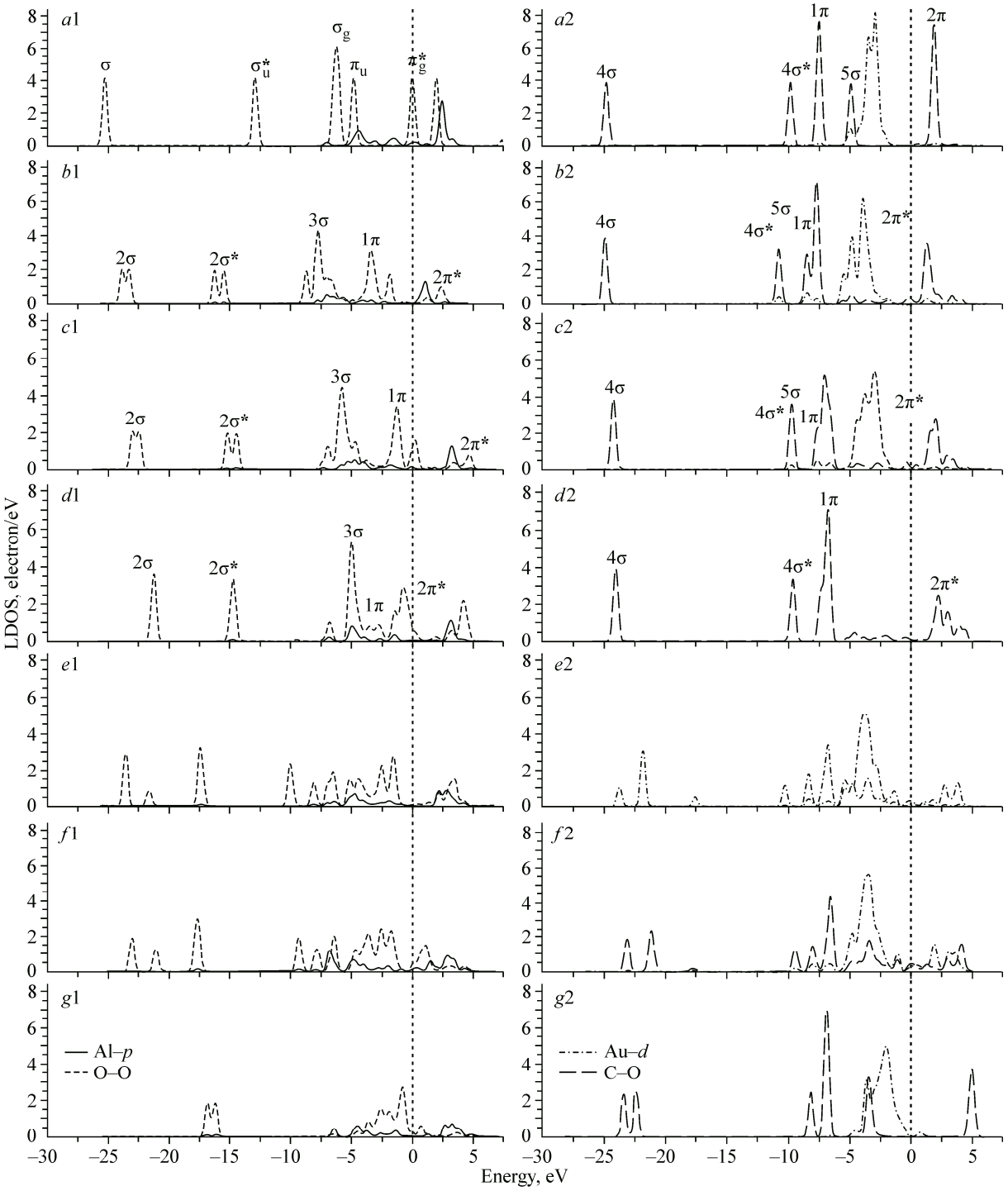

Fig. 4. LDOS projected onto O—O and C—O for CO oxidation on $AlAu_6$ *via* the proposed minimum-energy pathway

ment of the reaction; it requires an energy of 0.37 eV. The barrier along this pathway is 0.41 eV, which is lower that of path-1 (0.51 eV), demonstrating that the cooperation effect of second CO can prompt CO oxidation. The overall reaction is calculated to be exothermic (6.37 eV).

In this study, we found that the activation barrier of the determination rate of CO with the $AlAu_6$ cluster is lower than that of the pure Au_6^- cluster (0.78 eV) [31].

Analysis of the electronic state during CO oxidation. In addition, we also calculate the local density of states (LDOS) of the CO oxidation process for path-1 with the lowest energy barrier for the $AlAu_6O_2^*$ complex. Electronic LDOS of the system projected on the orbital for the adsorbed constructs of O_2 (left panel) and CO (right panel) species, as well as the *d* projected electron density of the bound Au and Al atoms, are depicted in Fig. 4. Fig. 4, *a* shows LDOS of isolated O_2, CO, and the $AlAu_6$ cluster; Fig. 4, *b* shows O_2 or CO adsorption on the $AlAu_6$ cluster; Fig. 4, *c*—*g* corresponds to LDOS of IM1, $TS_{1/2}$, IM2, $TS_{2/3}$, and IM3 configurations, respectively.

O_2 adsorption on the $AlAu_6$ cluster (Fig. 4, *b*1) causes the broadening of the antibonding O_2 $2\pi^*$ orbital, which strengthens the overlap with the *p* state of the Al atom, resulting in charge transfer from the Al atom to the adsorbed O_2 species. In Fig. 4, *b*2, adsorbed CO with more negative energies is compared with unabsorbed CO bands, which results in the overlap between the occupied 5σ orbital and unoccupied $2\pi^*$ orbital of CO with the Au *d* states[32]. As these interactions proceed (from Fig. 4, *c*1 to 4, *g*1), it can be seen that, from IM1 to $TS_{1/2}$, the orbitals clearly show stronger hybridization between the O and Al atoms (*p* orbital). As shown in Fig. 4, *e*1 (IM2), the π_g^* state is elevated to interact with the Al *p* state, from IM2 to $TS_{2/3}$, a pronounced broadening of the π_g^* state occurs at the dissociation of adsorbed O_2. As these interactions proceed (from Fig. 4, *c*2 to 4, *g*2), the antibonding $2\pi^*$ orbitals of CO species on the $AlAu_6$ cluster spread back and overlap with the Au *d* states. As shown in Fig. 4, *e*2 (IM2), a pronounced broadening can be found above the Fermi level. It is partially populated due to the back donation of Au *d* electrons and charge transfer between the unoccupied CO $2\pi^*$ orbital with the Au *d* states, as indicated by a slight increase in the C—O bond length [5]. Finally, as shown in Fig. 4, *g*, LDOS for the products are similar to those of absorbed O and the separated CO_2 gas phase on the $AlAu_6$ cluster.

Spin density distribution during CO oxidation. The analysis of spin density distributions provides direct information as to the relative importance of various resonance forms and is based on the DFT structures. Spin density distributions in the intermediates along the reaction paths found by the PBE /6-31G* calculation are presented in Fig. 5.

As for the difference electron density, similar qualitative conclusions can also be drawn for the spin density of the $AlAu_6$ cluster for CO oxidation (Fig. 5). For IM1 and IM4, the donor atoms directly attached to the metal carry the positive spin density and from there it is propagated through the carbonyl bonds with alternating signs. Some positive spin density is carried due to the polarization of the electron pair in a low-lying bonding molecular orbital centered mainly on the carbonyl group. For IM3 and IM4, since the Al atom experiences no spin delocalization, the atomic orbitals are spin-polarized and carry a negative spin density. The spin densities at the terminal gold atom of IM1 and IM3 have the same sign. The formation of the $AlAu_6O$—OCO complex (IM2) results in an increase of the oxygen hyperfine spin density, theoretical shortening of C—O, and lengthening of O—O. The Mulliken population shows that between the carbon and oxygen atom, oxygen coming from carbonyl has a negative value, which is –0.13. At the same time, the Mulliken population of O—O is 0.23.

CONCLUSIONS

In summary, in this work the catalytic properties of $AlAu_6$ clusters in CO oxidation are studied via a thorough DFT sampling of PES of the cluster systems. Three main general conclusions can be drawn from this analysis.

First, for O_2 and CO adsorption in the $AlAu_6$ cluster, the active sites would be first occupied by coming O_2 rather than CO, in view of its more negative BE than that of CO.

Second, even a simple reaction such as CO oxidation, led by a strong thermodynamic driving force and involving a limited number of chemical species, can occur through a variety of different mechanisms, ranging from CO assisted O_2 breaking and a successive CO reaction with top oxygen species to the formation and successive decomposition of a double carbonate adduct.

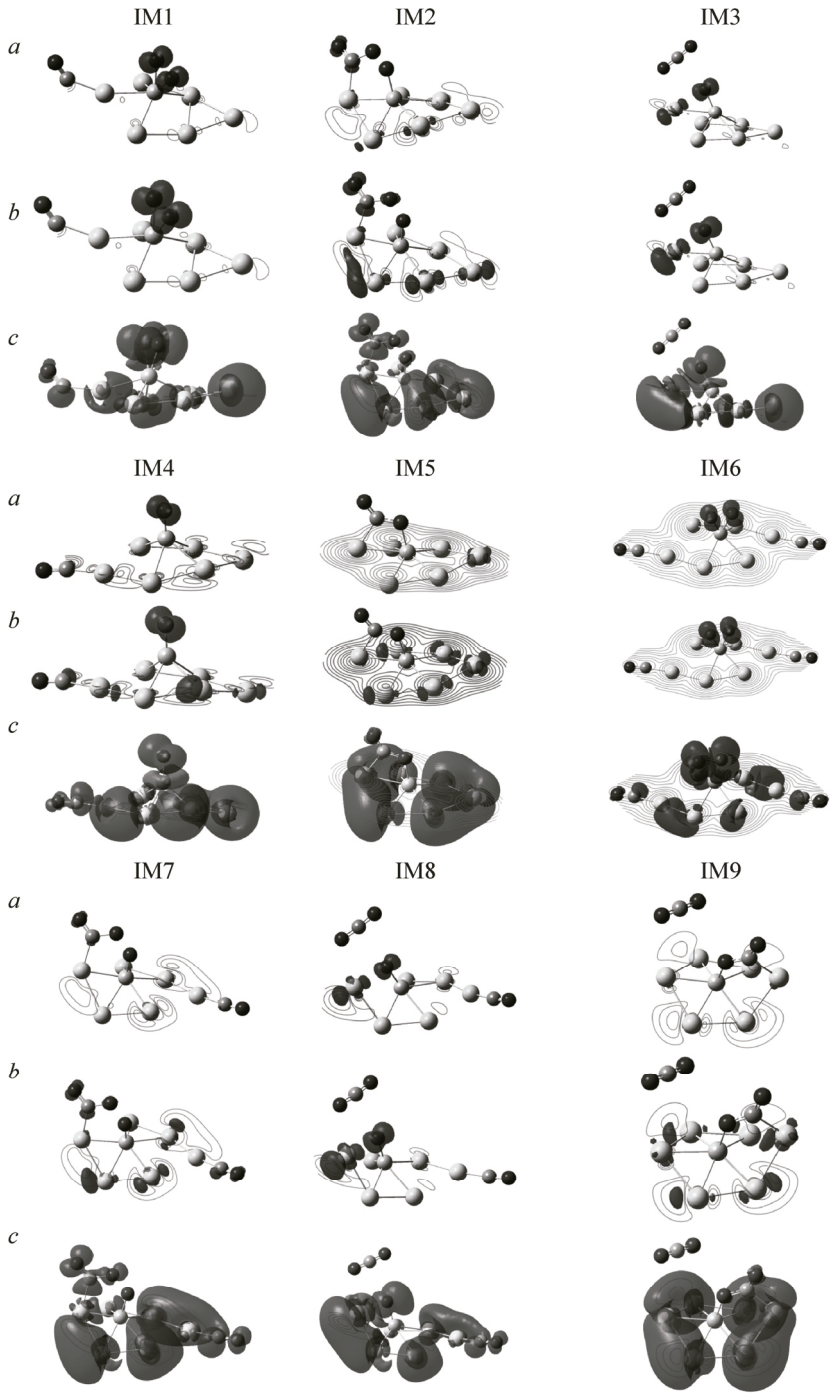

Fig. 5. Spin density distribution in PBE. Spin density contour values shown at 0.008 au (*a*), 0.004 au (*b*), and 0.0004 au (*c*)

Third, path-1 of CO with the $AlAu_6O_2^*$ complex has the lowest activation barrier (0.27 eV), which is lower by 0.51 eV as compared with the pure Au_6^- cluster. For the $AlAu_6O_2$ $(CO)_2$ complex, due to the structural distortion of the $AlAu_6$ cluster, the activation barrier of the determination rate is higher by 0.53 eV than that of the single CO molecule, which shows that the cooperation effect of second CO can go against CO oxidation. For the $Al@Au_6O_2$ $(CO)_2$ complex, the activation barrier of the determination rate is lower by 0.07 eV than that of the single CO molecule, demonstrating that the cooperation effect of second CO can prompt CO oxidation.

We believe that the present analysis opens interesting perspectives in the understanding and exploitation of heterogeneous subnanocatalysts while pointing to the need of efficient algorithms for the structural exploration to achieve a computational prediction.

This work was financially supported by the National Natural Science Foundation of China (grant No. 20603021), the Natural Science Foundation of Shanxi (grant No. 2013011009-6), the High School 131 Leading Talent Project of Shanxi, Undergraduate Training Programs for Innovation and Entrepreneurship of Shanxi Province (grant No. 105088, 2015537, WL 2015CXCY-SJ-O1), Shanxi Normal University (SD2015CXXM-80, WL2015CXCY-YJ-18) and Teaching Reform project of Shanxi Normal University(WL2015JGXM-YJ-13), Graduate student eduction innovation project in Shanxi Province.

REFERENCES

1. *Haruta M., Yamada N., Kobayashi T. et al.* // J. Catal. – 1989. – **115**. – P. 301.
2. *Green I.X., Tang W., McEntee M. et al.* // J. Am. Chem. Soc. – 2012. – **134**. – P. 12717.
3. *Liu X., Liu M.H., Luo Y.C. et al.* // J. Am. Chem. Soc. – 2012. – **134**. – P. 10251.
4. *Fujitani T., Nakamura I.* // Angew. Chem. – 2011. – **123**. – P. 10326.
5. *Shekhar M., Wang J., Lee W.S. et al.* // J. Am. Chem. Soc. – 2012. – **134**. – P. 4700.
6. *Lin R.J., Chen H.L., Ju S.P. et al.* // J. Phys. Chem. C. – 2012. – **116**. – P. 336.
7. *Zhang S., Guo S., Zhu H. et al.* // J. Am. Chem. Soc. – 2012. – **134**. – P. 5060.
8. *Sarina S., Zhu H., Jaatinen E. et al.* // J. Am. Chem. Soc. – 2013. – **135**. – P. 5793.
9. *Wang C.J., Kuang X.Y., Wang H.Q. et al.* // Comput. Theor. Chem. – 2012. – **1002**. – P. 31.
10. *Li Y.F., Mao A.J., Li Y. et al.* // J. Mol. Model. – 2012. – **18**. – P. 3061.
11. *Majumder C., Kandalam A.K., Jena P.* // Phys. Rev. B. – 2006. – **74**. – P. 205437-1.
12. *Zhang M., Chen S., Deng Q.M. et al.* // Eur. Phys. J. D. – 2010. – **58**. – P. 117.
13. *Zhang M., Yang S.B., Feng X.J. et al.* // Eur. Phys. J. D. – 2013. – **67**. – P. 11.
14. *Zhao G.F., Wang Y.L., Sun J.M. et al.* // Acta Phys.-Chim. Sin. – 2012. – **28**. – P. 1355.
15. *Yao W.Z., Liu B.T., Lu Z.H. et al.* // J. Phys. Chem. A. – 2013. – **117**. – P. 5178.
16. *Nhat P.V., Tai T.B., Nguyen M.T.* // J. Chem. Phys. – 2012. – **137**. – P. 164312-1.
17. *Lin L., Lieven P., Nguyen M.T.* // Chem. Phys. Lett. – 2010. – **498**. – P. 296.
18. *Wallace W.T., Whetten R.L.* // J. Am. Chem. Soc. – 2002. – **124**. – P. 7499.
19. *Rodríguez J., Feria L., Jirsak T. et al.* // J. Am. Chem. Soc. – 2010. – **132**. – P. 3177.
20. *Sun Q., Jena P., Kim Y.D. et al.* // J. Chem. Phys. – 2004. – **120**. – P. 6510.
21. *Fernández E.M., Ordejón P., Balbás L.C.* // Chem. Phys. Lett. – 2005. – **408**. – P. 252.
22. *Amft M., Johansson B., Skorodumova N.V.* // J. Chem. Phys. – 2012. – **136**. – P. 024312.
23. *Wang F., Zhang D., Xu X. et al.* // J. Phys. Chem. C. – 2009. – **113**. – P. 18032.
24. *An W., Pei Y., Zeng X.C.* // Nano. Lett. – 2008. – **8**. – P. 195.
25. *Stamatakis M., Christiansen M.A., Vlachos D.G. et al.* // Nano. Lett. – 2012. – **12**. – P. 3621.
26. *Chen H.T., Chang J.G., Ju S.P. et al.* // J. Comput. Chem. – 2009. – **31**. – P. 258.
27. *Kim H.Y., Han S.S., Ryu J.H. et al.* // J. Phys. Chem. C. – 2010. – **114**. – P. 3156.
28. *Gao Y., Shao N., Bulusu S. et al.* // J. Phys. Chem. C. – 2008. – **112**. – P. 8234.
29. *Negreiros F.R., Sementa L., Barcaro G. et al.* // ACS Catal. – 2012. – **2**. – P. 1860.
30. *Frisch M.J., Trucks G.W., Schlegel H.B. et al.* Gaussian 03, Revision C02; Gaussian, Inc. Pittsburgh, PA, 2003.
31. *Perdew J.P., Burke K., Ernzerhof M.* // Phys. Rev. Lett. – 1996. – **77**. – P. 3865.
32. *Peng C., Ayala P.Y., Schlegel H.B. et al.* // J. Comput. Chem. – 1996. – **17**. – P. 49.
33. *Gonzalez C., Schlegel H.B.* // J. Chem. Phys. – 1989. – **90**. – P. 2154.
34. *Gonzalez C., Schlegel H.B.* // J. Phys. Chem. – 1990. – **94**. – P. 5523.
35. *Segall M.D., Lindan P.J.D., Probert M.J. et al.* // J. Phys.: Condens. Matter. – 2002. – **14**. – P. 2717.
36. *Clark S.J., Segall M.D., Pickard C.J. et al.* // Kristallogr. – 2005. – **220**. – P. 567.
37. *Joe H., Kent M.E., Lineberger W.C.* // J. Chem. Phys. – 1990. – **93**. – P. 6987.
38. *Simard B., Hackett P.A.* // J. Mol. Spectrosc. – 1990. – **142**. – P. 310.
39. *Rosen B.* Spectroscopic Data Relative to Diatomic Molecules, Oxford University Press, New York, 1970.
40. *Gingerich K.A., Blue G.D.* // J. Chem. Phys. – 1973. – **59**. – P. 185.
41. *Morse M.D.* // Chem. Rev. – 1986. – **86**. – P. 1049.
42. *Zhang Y., Yang W.* // Phys. Rev. Lett. – 1998. – **80**. – P. 890.
43. *Lide D.R.* CRC Handbook of Chemistry, Physics, 55th edition, CRC Press: Cleveland, 1974.
44. *Lee H.M., Ge M., Sahu B.R. et al.* // J. Phys. Chem. B. – 2003. – **107**. – P. 9994.
45. *Blyholder G.* // J. Phys. Chem. – 1964. – **68**. – P. 2772.